JOURNAL OF AGRICULTURAL AND FOOD CHEMISTRY

Proteome Changes in Leaves of *Brassica napus* L. as a Result of *Sclerotinia sclerotiorum* Challenge

YUE LIANG, SANJEEVA SRIVASTAVA, MUHAMMAD H. RAHMAN, STEPHEN E. STRELKOV, AND NAT N. V. KAV*

Department of Agricultural, Food and Nutritional Science, University of Alberta, Edmonton, Alberta T6G 2P5, Canada

Sclerotinia stem rot, caused by the necrotrophic fungal pathogen *Sclerotinia sclerotiorum*, is a serious disease of canola (*Brassica napus* L.). To increase the understanding of the *B. napus*−*S. sclerotiorum* interaction, proteins potentially involved in mediating this interaction were identified and characterized. Upon infection of canola leaves by *S. sclerotiorum*, necrosis of host leaves was observed by 12 h and rapidly progressed during the later time points. These morphological observations were supported by microscopic study performed at different time points after pathogen challenge. Leaf proteins were extracted and analyzed by 2-DE, which revealed the modulation of 32 proteins (12 down- and 20 up-regulated). The identities of these proteins were established by ESI-q-TOF MS/MS and included proteins involved in photosynthesis and metabolic pathways, protein folding and modifications, hormone signaling, and antioxidant defense. Gene expression analysis of selected genes was performed by qRT-PCR, whereas the elevated levels of the antioxidant enzymes peroxidase and superoxide dismutase were validated by enzyme assays. To the authors' best knowledge, this is the first proteomics-based investigation of *B. napus*−*S. sclerotiorum* interaction, and the roles of many of the proteins identified are discussed within the context of this pathosystem.

KEYWORDS: Biotic stress; *Brassica napus*; glyoxalase; peroxidase; *Sclerotinia sclerotiorum*

INTRODUCTION

Canola (*Brassica napus* L.) is an economically important oilseed crop that is cultivated worldwide, including Canada and the United States. Sclerotinia stem rot, caused by *Sclerotinia sclerotiorum* (Lib.) de Bary, is one of the most serious diseases affecting canola and has the potential to significantly limit yields (*1*). In addition to being able to infect canola, *S. sclerotiorum* is a necrotrophic, generalist parasite capable of infecting approximately 400 plant species (*2*). In canola, outbreaks of Sclerotinia stem rot generally occur near the end of flowering period, late in the plant-growing season. Infection is initiated by airborne ascospores, which land on and infect the flower petals under favorable conditions (i.e., high moisture and high temperature); infected petals fall on leaves and leaf axils, from which the pathogen can grow into the host stem, forming lesions that may completely girdle the stem and cause plant death (*3*). Black sclerotia are eventually formed within the infected canola stems, which serve as a survival structure for *S. sclerotiorum* and as a source of inoculum in subsequent seasons.

The biochemical and molecular events occurring in host plant tissues during disease progression are not clear. In the past, research on the molecular aspects of pathogenicity of *S. sclerotiorum* mainly focused on the role of oxalic acid and cell-wall-degrading enzymes (CWDEs) such as glycosidase, pectinases, xylanases (*4*), and polygalacturonases (PGs) (*5*). The secretion of oxalic acid by *S. sclerotiorum* has been found to be an essential determinant of its pathogenicity in bean and sunflower (*6*), and the compound is considered to be a crucial pathogenicity factor produced by the fungus (*7*). In addition to oxalic acid, the pathogen also secretes CWDEs that can facilitate penetration and degradation of host cell walls (*8*). Among the CWDEs, PGs are pectinases that can degrade unesterified pectate polymers present in plant cell walls and for which important roles as virulence factors have been demonstrated in a few pathosystems (*9*). In addition, a recent analysis of the proteins secreted by this pathogen, the secretome, has revealed additional proteins that may be important during pathogenesis (*10*).

Although there are a number of papers in the literature that describe the importance of oxalic acid and CWDEs for infection and pathogenesis by *S. sclerotiorum*, there are very few studies describing detailed molecular changes that accompany infection in the host. In fact, only two papers are available in the literature that have employed genomics-based techniques to identify plant and fungal genes that are modulated during *B. napus*−*S. sclerotiorum* interactions (*11, 12*). The first was an expressed sequence tag (EST) analysis of fungal genes expressed during growth in pectin medium or in infected plant tissue, which revealed a number of fungal genes important for pathogenesis (*11*). The second study involved an investigation into changes

* Corresponding author [telephone (780) 492-7584; fax (780) 492-4265; e-mail nat@ualberta.ca].

10.1021/jf073012d CCC: $40.75
Published on Web 02/22/2008

in gene expression in the host (canola) tissue accompanying *S. sclerotiorum* infection and which identified a number of plant genes that were modulated during infection (*12*). Although genomics-based investigation of host−pathogen interactions can provide valuable information into the changes in gene expression, an investigation into changes in protein abundance is also important, in order to identify those proteins that are essential during such interactions. This is because there is often a poor correlation between transcript and protein abundance (*13*). In this postgenomic era, proteomics-based approaches employing two-dimensional gel electrophoresis (2-DE) and mass spectrometry (MS) are widely used to investigate various plant processes, including biochemical and physiological responses to abiotic or biotic stresses at the proteome level (*14*−*18*).

The identification and characterization of host proteins having levels affected by pathogen challenge is important in elucidating their roles in mediating the host response and is one of our long-term objectives. In this paper, we describe the changes in the leaf proteome of *B. napus* accompanying infection by *S. sclerotiorum*, which was investigated using 2-DE and tandem MS. We have identified 32 proteins having levels that were modulated significantly at various time points after pathogen challenge, and the roles of these proteins are discussed within the context of the stem rot pathosystem.

MATERIALS AND METHODS

Plant Material and Fungal Cultures. *B. napus* and *Arabidopsis thaliana* seeds were sown in plastic trays with 32 cell packs containing Metro Mix 290 (Grace Horticultural products, Ajax, ON, Canada). Plants were grown in the greenhouse (16 h photoperiod, 22 °C day/18 °C night) for 18 days. *A. thaliana* seeds were vernalized by placing the trays in a dark room at 4 °C for 2 days. All plants were placed in a humidity chamber for 24 h prior to inoculation. Cultures of *S. sclerotiorum* were grown on potato dextrose agar (PDA; Becton Dickinson, Columbia, MD) and incubated at room temperature for 3 days. Actively growing mycelia from the edge of the colony were subcultured onto fresh PDA media and grown for an additional 2 days, after which mycelial plugs (5 mm) were excised from the cultures and used to inoculate leaves of *B. napus* (two true leaves) and *A. thaliana* (all of the true leaves), which were gently wounded by scratching with a pipette tip. Similarly, control leaves were wounded and inoculated with PDA plugs alone. After inoculation, plants were returned to the humidity chamber for an additional 24 h, after which they were transferred to and maintained in the greenhouse. Shoot samples from control and inoculated plants were harvested at 6, 12, 24, 36, and 48 h after inoculation, flash frozen in liquid nitrogen, and stored at −80 °C. Three independent biological replicates were performed for each treatment; each biological replicate consisted of 10 plants at each time point.

Histology. The infected leaf material and controls were cut into small (5 × 10 mm) sections, containing a portion of the wounded region, and fixed at 4 °C overnight in 50 mM phosphate buffer (pH 7.2) containing 4% paraformaldehyde by vacuum infiltration. Subsequently, they were dehydrated in a graded ethanol series, changed to toluene, and infiltrated with Paraplast (Fisher, Pittsburgh, PA). Paradermal sections (6 μm thickness) were cut, affixed to slides, deparaffinated with toluene (two changes of 5 min each), rehydrated to 50% ethanol, and stained with Aniline Blue in lactophenol (*19*) for 10 min. Stained sections were rinsed with water (three changes of 3 min each), counterstained with acidified Eosin Y (*20*) for 1 min, dehydrated, and mounted with DPX (Electron Microscopy Sciences, Hatfield, PA) mounting medium. The sections were viewed with a Leica DM *RXA* microscope (Leica Microsystems, Wetzlar, Germany) and photographed using an Optronics digital camera with Macrofire software (Optronics, Goleta, CA).

Protein Extraction. Pooled *B. napus* leaves (∼300 mg) were ground to a fine power in liquid nitrogen and then resuspended in 1.5 mL of actone containing 10% trichloroacetic acid (TCA; Fisher, Fair Lawn, NJ) and 0.07% dithiothreitol (DTT, Fisher). After incubation at −20 °C for 1 h, the suspension was vortexed and centrifuged (18000*g*, 15 min, 4 °C). After removal of the supernatant, pellet was resuspended in 1 mL of ice-cold acetone containing 0.07% DTT and centrifuged as described above. This washing step was repeated an additional four times. The washed pellets were dried for 10 min in a Speedvac (Hetovac VR-1; Heto Laboratory Equipment A/S, Birkerod, Denmark) and resolubilized in 400 μL of rehydration/sample buffer (Bio-Rad, Mississauga, ON, Canada) containing 0.1% tributylphosphine (TBP, Bio-Rad) and incubated overnight at 4 °C. After incubation, the samples were vortexed vigorously and centrifuged as described above, and the supernatants were transferred to fresh tubes and stored at −20 °C until analysis by electrophoresis. The protein samples were prepared twice from each three independent biological replicates of leaf tissue for a total of six samples for each time point. Protein concentrations were determined using a modified Bradford assay (*21*) with bovine serum albumin (BSA; Pierce Biotechnology, Rochford, IL) as the standard.

Two-Dimensional Electrophoresis. Isoelectric focusing (IEF) of extracted protein in the first dimension and separation by sodium dodecyl sulfate−polyacrylamide gel electrophoresis (SDS-PAGE) in the second dimension were performed as previously described (*16*). Briefly, 17 cm IPG (pH 4–7, Bio-Rad) strips were rehydrated overnight with 400 μg of protein in 300 μL of rehydration/sample buffer. IEF was preformed using a PROTEAN IEF cell (Bio-Rad) to separate proteins based on difference in isoelectric points. The focused IPG strips were equilibrated in 5 mL of equilibration buffer containing 6 M urea, 2% SDS, 0.37 M Tris-HCl, pH 8.8, 20% glycerol, and 130 mM DTT for 10 min and then incubated in the same buffer containing 135 mM iodoacetamide (IAA) for 10 min. The equilibration steps in both buffers were performed twice. For the separation of the focused proteins in the second dimension, SDS-PAGE was performed using a PROTEAN II XI cell (Bio-Rad). The separated proteins were stained using a Colloidal Coomassie Blue Staining Kit (Invitrogen, Carlsbad, CA) per the manufacturer's instructions.

2-D Gel Analysis and Protein Identification. Images of the 2-D gels were recorded using a GS-800 calibrated densitometer (Bio-Rad) and analyzed using PDQuest 2-D analysis software (version 7.3.1, Bio-Rad). A matchset was created from images of 12 gels (for each time point), which consisted of two extractions from each of the three biological replicates for the control and inoculated plants at each time point. Analysis of the 2-D gels was performed using the automated detection and matching tools of the PDQuest software, and artifacts were removed by manual refinement of the matched spots. Replicate groups for control and inoculated gels were created and analyzed using the Student's *t*-test feature of the software, in order to identify those spots that showed statistically significant ($p < 0.05$) differences in intensities. The quantities of these significantly altered spots were determined using the spot quantification tool, and fold-changes were calculated. Among the statistically significant ($p < 0.05$) spots, only those that showed reproducible changes (up- or down-regulation) in all of the replicates were selected for further analysis using tandem MS. Electrospray ionization quadrupole time-of-flight tandem mass spectrometry (ESI-q-TOF MS/MS) experiments were performed at the Institute for Biomolecular Design (IBD), University of Alberta, using a Micromass Q-TOF-2 mass spectrometer (Micromass, Manchester, U.K.) as described previously (*10*). Data-dependent MS/MS acquisition was performed for peptides with a charge state of two or three, and the data were processed using the Mascot (Matrix Science Inc., Boston, MA) search engine and the NCBI nonredundant protein database. Parameters that were utilized for the Mascot search included carbamidomethylation of cysteine, possible oxidation of methionine, and one missed cleavage per peptide.

Quantitative Real-Time PCR. Primers and probes were designed using Primer Premier 3 software (Applied Biosystems Inc., Foster City, CA) to generate amplicons approximately 60 bp in size and are listed in **Table 1**. Total RNA was extracted from control and inoculated pooled leaf samples for all of the time points using RNeasy Plant Mini Kit (QIAGEN, Mississauga, ON, Canada). During RNA extraction, an RNase-free DNase (Qiagen) treatment was included to ensure complete removal of contaminating genomic DNA. First, strand cDNA was synthesized by reverse transcription of 50 ng total RNA using the iScript

Table 1. Sequences of the Primers and Probes Used for qRT-PCR Analysis

gene	accession no.	primers and probe
uroporphyrinogen decarboxylase (*A. thaliana*)	AY035057	F-5′-TGGGCAACCGAGCTTAGC-3′ R-5′-GAGAGGTAGGTTTGGGTGAGTTTG-3′ P-5′-TGGATTTTGAGGAGTTTAGCT-3′
ATPase (*A. thaliana*)	NM_100523	F-5′-TGTTGGTGGACTCGGTGGTA-3′ R-5′-CAAACCGGTGATCTGTTGCA-3′ P-5′-AGCTGCCGAAGAAG-3′
peroxidase (*A. thaliana*)	NM_111480	F-5′-TCCACCACGCCATTGTCA-3′ R-5′-TAGGCACATGCTGCTGTGAAC-3′ P-5′-AGAAAGTCGTCATCTTTGGT-3′
triosephosphate isomerase (*A. thaliana*)	NM_127687	F-5′-CGCTCCCCCAGAGGTGTT-3′ R-5′-TTCCTCCAACGAAAAACTTTCC-3′ P-5′- TGCCATGGCTGGATC-3′
fructose-bisphosphate aldolase (*A. thaliana*)	NM_120057	F-5′-GCGGTTTGGTTCCGATTGT-3′ R-5′-TCAATGTCGTGTTCTCCATCCA-3′ P-5′- AGCCAGAGATCTTG-3′
glyceraldehyde 3-phosphate dehydrogenase (*A. thaliana*)	ATHCPGAPBA	F-5′-GGAAGCTGTTGGAAGTGGAGAT-3′ R-5′- TCATCAGCCGGGTTTGTCTT-3′ P-5′- 6FAM-CTTTGGAGGATTTCTG-3′
glyoxalase I (*A. thaliana*)	NM_105396	F-5′- AAGTTATGCTCCGTGTTGGTGAT-3′ R-5′- TCCATTCCAAAAGCCTTCTCA-3′ P-5′- CGATAGGGCCATAAAG-3′
actin (*B. napus*)	AF111812	F-5′- TGGGTTTGCTGGTGACGAT-3′ R-5′- TGCCTAGGACGACCAACAATACT-3′ P-5′- CTCCCAGGGCTGTGTT-3′
actin (*A. thaliana*)	AY120779	F-5′- GCCATTCAGGCCGTTCTTT-3′ R-5′- ATCGAGCACAATACCGGTTGT-3′ P-5′- TCTATGCCAGTGGTCG-3′

cDNA synthesis kit (BioRad). Quantitative real-time PCR (qRT-PCR) was performed using TaqMan technology and the ABI PRISM 7700 (Applied Biosystems) DNA Sequence Detection System as previously described (*22*). qRT-PCR reactions were performed using 2 μL of 5 × diluted cDNA as template, 22.5 pmol of primers, 5 pmol, of probe, and 1× TaqMan PCR Master Mix (Roche, Branchburg, NJ) in a reaction volume totaling 20 μL. The relative expression of the various genes was calculated using the delta−delta method, employing the following formula: relative expression $= 2^{-[\Delta Ct\ sample - \Delta Ct\ control]}$ (*23*). For all qRT-PCR experiments, the actin gene was used as the endogenous control. The relative expression in inoculated sample was normalized against the expression level in control samples, which was considered as 1. qRT-PCR reactions for samples from each biological replicate were performed in duplicate, and the experiment was repeated at least twice for all time points.

Peroxidase (POD) and Superoxide Dismutase (SOD) Assays. Crude leaf extracts were prepared for the assay of POD and SOD activities. Fresh, pooled leaves (~200 mg) from control (mock-inoculated), inoculated, and untreated (without wounding and inoculation) plants were ground in 1 mL of sodium phosphate buffer (60 mM, pH 7.0) and transferred to 1.5 mL tubes. The homogenates were centrifuged (20000*g*) for 15 min at 4 °C and the supernatants removed and used for POD and superoxide dismutase (SOD) assays. POD was assayed as described by Benkeblia and Shiomi with minor modifications (*24*). The reaction mixture (10 μL of 45 mM guaiacol, 10 μL of 200 mM H_2O_2, and 180 μL of 65 mM sodium phosphate buffer, pH 6.5) was mixed with 10 μL of crude enzyme extract, and the absorbance was immediately measured at 430 nm using a spectrophotometer. After incubation at room temperature for 10 min, the absorbance was measured again. One unit of enzyme activity was defined as a change in absorbance of 0.01 min^{-1} (*24*). POD enzyme assay was performed using leaf samples from three independent biological replicates, and the whole experiment was repeated at least two times.

SOD enzyme activity was assayed by measuring the photochemical reduction of nitro blue tetrazolium (NBT) (*25*) in a reaction mixture containing 50 mM phosphate buffer (pH 7.8), 13 mM methionine, 75 μM NBT, 2 μM riboflavin, 0.1 mM EDTA, and 0–20 μL of enzyme extract in a total volume of 200 μL. To avoid delays in performing enzyme assays, ELISA plates were used to accommodate multiple samples. The reaction mixture (except riboflavin) was added to all of the wells, riboflavin was added last, and the plate was placed 3 cm below a light source (two 34 W fluorescent lamps) for 10 min; the reaction was terminated by switching off the light source. The plates were covered with a black cloth until the absorbance was recorded at 560 nm and compared with the maximum absorbance in wells without the enzyme. The amount of enzyme extract corresponding to 50% inhibition of maximum color formation in enzyme-free extracts was considered to be one enzyme unit (*26, 27*).

Statistical Analysis. Statistical analyses of proteome level changes were performed using the Student's *t*-test feature of PDQuest software as described earlier and significance ($p < 0.05$) was calculated as per the manufacturer's instructions. Analysis of POD and SOD activity and qRT-PCR results was performed using analysis of variance (ANOVA) with the mixed model procedure of SAS version 9.1 (Statistical Analysis System; SAS Institute Inc., Cary, NC).

RESULTS AND DISCUSSION

Morphology and Histology. The appearance of *B. napus* leaves at various time points (6, 12, 24, 36, and 48 h) after inoculation with *S. sclerotiorum* is shown in **Figure 1**. Symptoms of leaf necrosis began to appear 12 h after inoculation, which spread relatively rapidly by 24 h, suggesting that rapid invasion of the host tissue occurs between 12 and 24 h. To examine the invasion of leaf by the fungus, we examined the uninoculated and inoculated leaves using light microscopy at

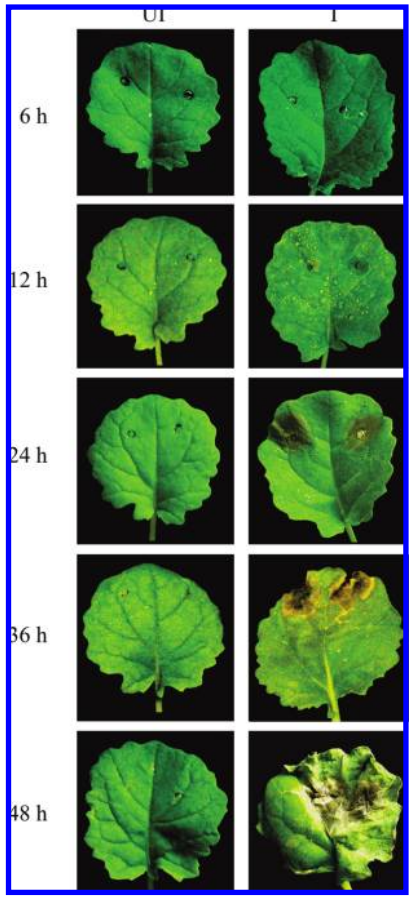

Figure 1. Appearance of *Brassica napus* leaves inoculated with *Sclerotinia sclerotiorum*. Leaves are shown 6, 12, 24, 36, and 48 h after inoculation with the pathogen or mock-inoculation with an agar plug only. The labels UI and I refer to control and inoculated leaves, respectively.

the various time points indicated above. These results are illustrated in **Figure 2**. At 6 h after inoculation, there was no visible growth of the fungal mycelia in the host tissue. Although no mycelia were detectable, the cells in close proximity to the inoculation point demonstrated characteristics different from those of the cells that are distal to the infection site. These cells, especially the chloroplasts and the starch granules contained within them, and the adjacent cytoplasm stained more intensely with Aniline Blue and appeared darker compared to the cells more distal to the inoculation point. The control plant cells stained less intensely, and this phenomenon was also observed in all successive time points. The greater staining intensity of the cells may have been an indication of biochemical/ physiological changes occurring prior to the actual infection process. At 12 h after inoculation, fungal mycelia, stained pink with Eosin Y, could be seen in close proximity to the host tissue (**Figure 2**), indicating the possible initiation of the infection process and the gradual establishment of the pathogen within the host. Once again, the mesophyll cells in close proximity to the fungal mycelia stained more intensely with Aniline Blue, whereas the cells in the noninfected region were lighter in color and had a purplish hue. Changes in histochemical properties, along with the accumulation of crystalline structures, preceding invasion of bean tissue by fungal mycelia have previously been reported (*28*). By 24 h after inoculation, the pathogen was well established in the host tissue, and extensive mycelial growth was observed. The host tissue developed necrosis, and empty spaces in the tissue resulting from cell lysis could also be observed, which was also evident at 36 and 48 h after inoculation (**Figure 2**). Our histological findings correlate well with the observed phenotypic changes after pathogen challenge at the various time points (6, 12, 24, 36, and 48 h). We observed no visible damage to the leaf tissue at 6 h, and the first symptoms appeared at 12 h (**Figure 1**). The amount of fungal mycelia detectable in the host tissue increased at 24, 36, and 48 h after inoculation, as did the severity of macroscopic disease symptoms (**Figures 1** and **2**).

Protein Changes and Identification of *S. sclerotiorum*-Responsive Proteins. Changes in the leaf proteome of *B. napus* resulting from challenge by *S. sclerotiorum* were characterized using 2-DE at 6, 12, 24, 36, and 48 h after inoculation, and representative images are shown in **Figure 3**. Two protein extractions were performed from each of the three biological replicates, for a total of six independent protein samples for each time point, all of which were characterized by 2-DE. Gels ($n = 6$) for each time point were grouped and compared with gels of protein extracted from control (uninoculated) leaves using the Student's *t*-test feature of the PDQuest software (Bio-Rad). A total of 32 spots demonstrated significant ($p < 0.05$) differences (12 decreased and 20 increased) in intensities in samples from the inoculated leaf material, among which 4, 6, 8, 6, and 8 protein spots were identified at 6, 12, 24, 36, and 48 h after inoculation, respectively (**Figure 3**). All of the proteins showing statistically significant ($p < 0.05$) changes in intensities after pathogen challenge were subsequently identified by MS/MS analysis, and their identities are presented in **Table 2**. For most of the protein spots, a single protein was identified; however, for a few spots (9, 27, 28, and 29), multiple identities were obtained (**Table 2**). In those cases, the molecular masses and/or isoelectric points were very close, making the unambiguous identification of these spots impossible. In addition, one spot (spot 7; **Table 2**), for which the score was below the threshold value, generated the same identity after repeated MS/MS analysis and was therefore included among the proteins identified. We have grouped the identified proteins on the basis of their functional roles, which are discussed in detail in subsequent sections.

Functional Classification of Identified Proteins. As indicated earlier, the proteins identified in this study as being significantly ($p < 0.05$) affected by *S. sclerotiorum* challenge were grouped according to their known intracellular functions (**Figure 4A**). It is evident that a large portion (33%) of the proteins have roles in photosynthesis and carbon metabolism. The second largest group of proteins (15%) was identified as those involved in protein folding and post-translational modifications, whereas 12% could not be classified on the basis of available information. Other major categories comprised of proteins involved in hormone biosynthesis and signaling (9%), protein synthesis (9%), energy metabolism (3%), chloroplast biogenesis (6%), nitrogen metabolism (6%), lipid metabolism (3%), and antioxidant defense (3%). The remainder of our discussion will focus on the role of proteins involved in (1) photosynthesis and metabolic pathways, (2) protein folding and modifications, (3) hormone signaling, and (4) antioxidant defense, because these proteins may have significant and important roles mediating plant responses to the pathogen.

Metabolism. A number of proteins identified in our study are known to be involved in carbon metabolism, including spots identified (**Figure 3**; **Table 2**) as ribulose-1,5-bisphosphate carboxylase/oxygenase (rubisco; spots 8 and 31), rubisco activase (RCA; spots 27 and 28), and phosphoribulokinase (PRK; spot 5). These proteins were up-regulated following inoculation. In contrast, protein spots identified as glyceralde-

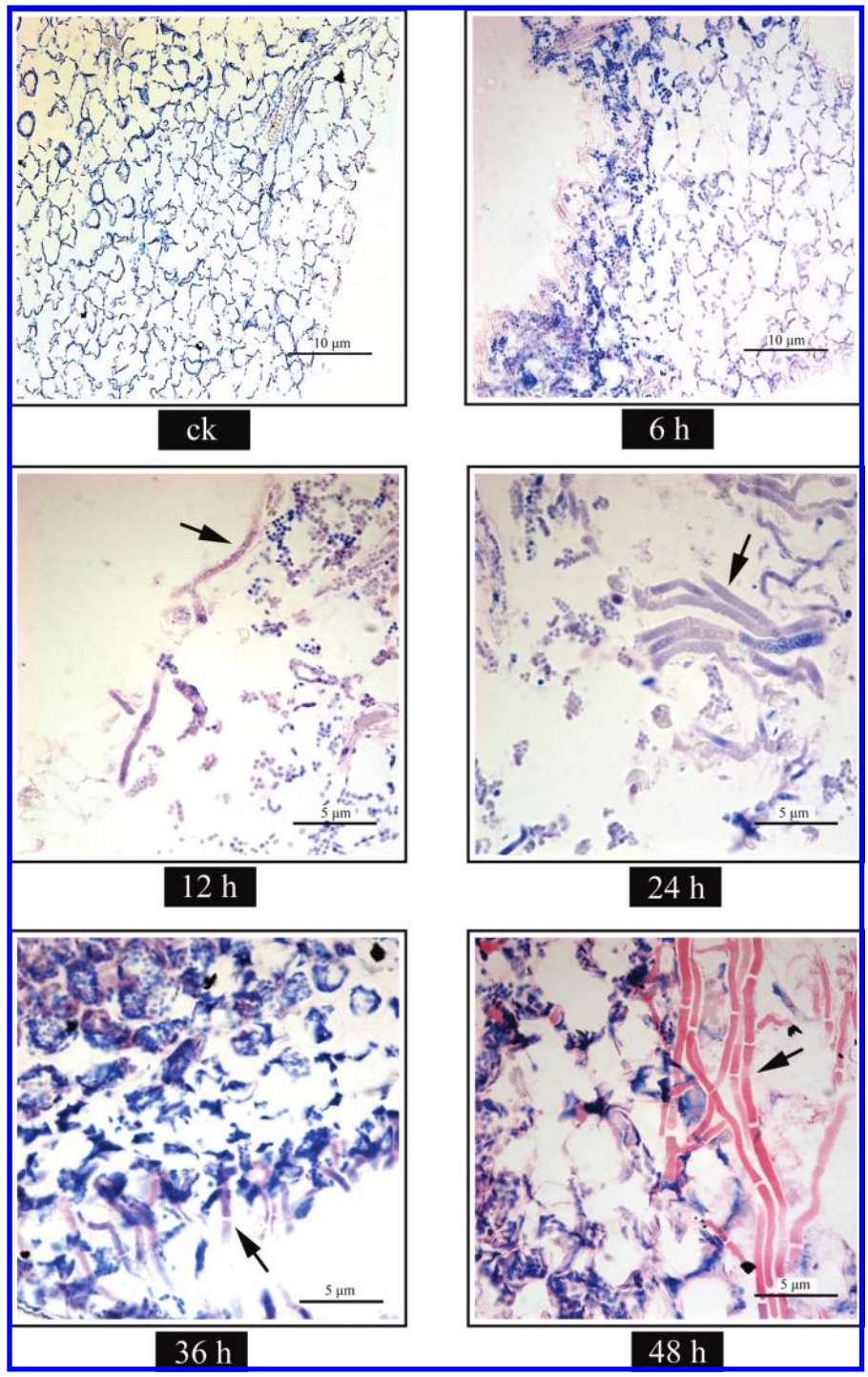

Figure 2. Light microscopy examining the invasion of *B. napus* leaves by *S. sclerotiorum* at various time points (6, 12, 24, 36, and 48 h) following inoculation along with uninoculated control (ck). Six micrometer thick paradermal sections of paraffin-embedded leaf tissue was stained with Aniline Blue in lactophenol and counterstained with Eosin Y. No fungal invasion (6 h), initiation of infection (12 h), and pathogen establishment and extensive mycelial growth (24–48 h) are apparent in these images. Arrows in the images point to fungal mycelia.

hyde-3-phosphate dehydrogenase (GAPDH; spot 17), fructose bisphosphate aldolase (FBPase; spots 15 and 24), triosephosphate isomerase (TPI; spot 3), and malate dehydrogenase (MDH; spot 4) show down-regulation following pathogen challenge (**Figure 3**; **Table 2**).

Rubisco catalyzes the carboxylation and oxygenation of ribulose bisphosphate in the Calvin and photorespiratory cycles, respectively (*29*). Rubisco is one of the key and unique catalysts of the Calvin cycle, one of the central steps in the global carbon cycle (*30*). Rubisco activase (RCA), a nuclear-encoded chloroplast protein, which removes inhibitors from its catalytic sites, alters its conformation and activates rubisco *in vivo* (*31, 32*), and our proteome analysis also revealed an increase in intensities of two spots identified as RCA at 48 h after pathogen challenge. It is important to indicate at this point that spots 27 and 28, which were both identified as RCA, also generated an additional hit each (**Table 2**) and, therefore, it is possible that these spots may not be RCA. However, for spot 28, the Mascot score for the second hit is considerably lower than that of the first hit, which was for RCA. In addition, spot 11 (**Figure 3**; **Table 2**), which was identified as an unnamed protein, exhibited 98% homology with rubisco (data not shown). Our results thus

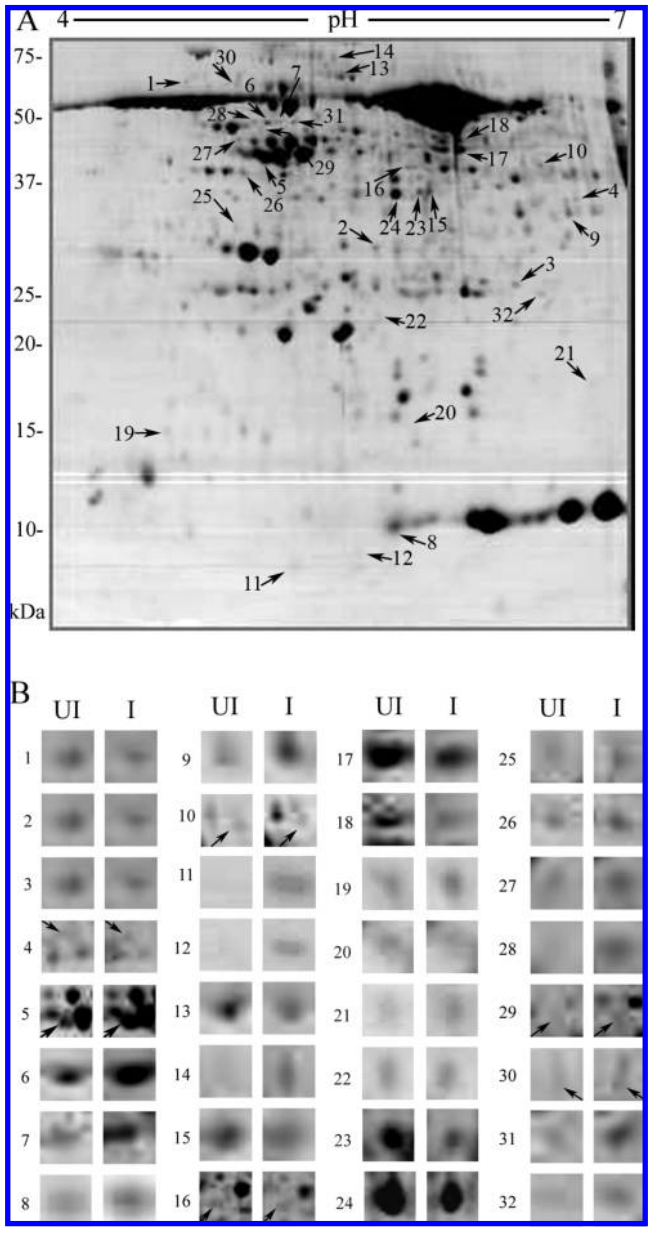

Figure 3. Proteome level analysis of *B. napus* leaves in response to inoculation with *S. sclerotiorum*: (**A**) representative image of *B. napus* leaf proteins separated by 2-DE and visualized with Coomassie Blue [protein spots, selected for MS/MS analysis, having intensities that were altered significantly ($P < 0.05$) as a result of pathogen challenge are indicated by arrows and numbers]; (**B**) closer view of spots showing significant changes.

indicate that rubisco, and perhaps RCA as well as PRK, which are involved in catalyzing reactions (PRK and rubisco) or activating enzymes (RCA) involved in the first stage of the Calvin cycle, may be increased as a result of *S. sclerotiorum* infection.

However, our studies also revealed a pathogen-induced decrease in the intensities of other enzymes involved in the Calvin cycle, including GAPDH, FBPase, and TPI (**Table 2**). The subunit of the plastidic form of GAPDH, which was found to be down-regulated ~3-fold at 24 h after inoculation (spot 17; **Figure 3**; **Table 2**), participates in the NADPH-dependent conversion of 1,3-bisphosphate glyceric acid to glyceraldehyde-3-phosphate (GAP). GAP and its isomer dihydroxyacetone phosphate (DHAP) are utilized in the biosynthesis of fructose 1,6-bisphosphate by FBPase, which was also observed to decrease in intensity at 24 h (spot 15; **Figure 3**; **Table 2**), suggesting that the formation of hexose phosphate by the Calvin cycle may be reduced due to pathogen infection. In addition, spot 23 (**Figure 3**; **Table 2**) also exhibited an approximate 2-fold decrease in intensity and generated peptides that matched FBPase. Incidentally, TPI, which catalyzes the isomerization of GAP to DHAP, was also observed to decrease in intensity, albeit to a lesser extent (1.8-fold) and at an earlier time point (6 h) (spot 3; **Figure 3**; **Table 2**). Our results suggest that even though CO_2 fixation by rubisco may be increased in infected leaf tissue, subsequent reactions may be slowed as a result of a decrease in the levels of GAPDH, TPI, and FBPase. The exact significance of the *S. sclerotiorum*-induced increase in PRK and rubisco and the concomitant decrease in GAPDH, TPI, and FBPase are at the present time unclear.

Proteins are involved in energy metabolism and transport, including ADP-glucose pyrophosporylase (AGPase; spot 32; **Figure 3**; **Table 2**). AGPase produces ADP-glucose, a substrate for starch synthesis in plants (*33*), and it has been suggested that this enzyme is tightly regulated by 3-phosphoglycerate and inorganic phosphate (*34*). The other protein that also increased following pathogen challenge was uroporphyrinogen decarboxylase (UROD; spot 10; **Figure 3**; **Table 2**). UROD is a central enzyme in the tetrapyrrole biosynthetic pathway, which may have a role in mediating plant responses to pathogens (including tolerance). This suggestion is supported by the fact that antisense of UROD in tobacco confers increased tolerance to tobacco mosaic virus (TMV) (*35*).

Nitrogen nutrition is critical to plants, and nitrogen deficiency often results in increased susceptibility to diseases (*36*). Proteins involved in nitrogen metabolism, including glutamine synthetase (GS; spot 27) and glutamate ammonia ligase (spot 29; **Figure 3**; **Table 2**), were identified in our studies, although as the number two hit in both instances. GS/glutamate ammonia ligase is a key enzyme that is responsible for the assimilation of ammonia, catalyzing the reaction of NH_3, ATP, and L-glutamate to phosphate, ADP, and L-glutamine (*37*). Increased expression of GS during disease progression has been demonstrated in many host−pathogen interactions. These include pathosystems involving *Stylosanthes guianensis*−*Colletotrichum gloeosporioides* (*38*), *B. carinata*−*Leptosphaeria maculans* (*15*), *Triticum aestivum*−*Puccinia triticina* (*39*), and *T. aestivum*−*Fusarium graminearum* (*18*). Furthermore, the inhibition of GS activity by a phytotoxin produced by *Pseudomonas syringe* (*40*) suggests a crucial role for this enzyme in mediating host−pathogen interactions. Because leaf necrosis affects nitrogen metabolism from assimilation to remobilization, which is normally accompanied by an elevation of GS (*41*), it is possible that the increased level of GS observed in this study may positively affect the remobilization of nitrogen from those necrotic tissues.

Chaperones and Post-translational Modification of Proteins. Molecular chaperones are a family of cellular proteins that mediate the correct folding of other proteins, but they themselves are not components of the final structures (*42*). Under various stress conditions, chaperones play an important role in restoring the native conformation of unfolded proteins (*43*). Our proteomics investigation revealed the identity of a few proteins with chaperone activity. These included protein disulfide isomerase (PDI; spot 1) and chaperonin precursor (spot 13; **Figure 3**; **Table 2**). PDI acts as a molecular chaperone in maintaining proper protein folding and, besides processing disulfide isomerase activity, catalyzes the refolding of many proteins (*44*). Within the context of plant responses to pathogens,

Table 2. Summary of the Differentially Expressed Proteins Identified from Susceptible Leaf Tissue of *Brassica napus* after Inoculation with *Sclerotinia sclerotiorum*

				ESI-q-ToF				
spot	time point (h)	protein identity	MS/MS/PM[a] (%)	score[b]	peptide sequence (charge state)	accession no.[c]	M_r/pI	fold change
1	6	ATPDIL1-1; electron transporter/ isomerase/ protein disulfide isomerase [*Arabidopsis thaliana*]	3/3	106/50	K.IDASEETNR.E (2^+) K.IDASEETNR.E (2^+) K.AVQEYNGPR.E (2^+)	gi 15219086	55852/ 4.81	1.71 ± 0.26 ↓
2	6	unknown protein [*A. thaliana*]	4/10	114/49	R.TGQIVYK.K (2^+) K.MKPGFDPTK.G (2^+) K.MKPGFDPTK.G (2^+) K.DDELLQTDTK.T (2^+)	gi 18413869	27143/ 6.19	1.52 ± 0.12 ↓
3	6	triosephosphate isomerase 1 [*Zea mays*]	4/10	175/49	K.VIACVGETLEQR.E (2^+) R.EAGSTMDVVAAQTK.A (2^+) R.EAGSTMDVVAAQTK.A (2^+) R.EAGSTMDVVAAQTK.A (2^+)	gi 168647	27236/ 5.52	1.79 ± 0.25 ↓
4	6	malate dehydrogenase/ oxidoreductase [*A. thaliana*]	2/6	128/49	K.LFGVTTLDVVR.A (2^+) R.TQDGGTEVVEAK.A (2^+)	gi 15232468	36024/ 8.30	1.38 ± 0.15 ↓
5	12	ATP binding/kinase/ phosphoribulokinase/ uridine kinase [*A. thaliana*]	2/5	71/50	R.KLTCSYPGIK.F (2^+) K.FYGEVTQQMLK.H (2^+)	gi 15222551	44721/ 5.71	1.54 ± 0.20 ↑
6	12	JR1 [*A. thaliana*]	2/3	69/38	K.FDYEKDGK.I (2^+) K.IVSLEHGK.Q (2^+)	gi 30684083	48524/ 5.12	1.89 ± 0.34 ↑
7	12	JR1 [*A. thaliana*]	1/1	35/37	K.FDYEKDGK.I (2^+)	gi 30684083	40524/ 5.12	2.17 ± 0.30 ↑
8	12	ribulose bisphosphate carboxylase [*Brassica napus*]	4/16	124/50	R.EHGSTPGYYDGR.Y (3^+) R.EHGSTPGYYDGR.Y (2^+) K.TEYPNAFIR.I (2^+) R.IIGFDNNR.Q (2^+)	gi 17850	20499/ 8.23	1.81 ± 0.34 ↑
9	12	ferredoxin-NADP$^+$ reductase [*A. thaliana*]	3/12	124/50	R.EGQSVGVIADGIDK.N (2^+) K.DPNATVIMLATGTGIAPFR.S (3^+) K.DNTFVYMCGLK.G (2^+)	gi 8778996	39147/ 8.65	2.08 ± 0.38 ↑
		chain B, wild-type pea Fnr	2/7	75/50	R.LVYTNDAGEVVK.G (2^+) K.DNTFVYMCGLK.G (2^+)	gi 4930124	35060/ 6.54	
10	12	putative uroporphyrinogen decarboxylase [*A. thaliana*]	7/10	110/38	K.SYQTLCEK.Y (2^+) K.SYQTLCEK.Y (2^+) K.SYQTLCEK.Y (2^+) K.SYQTLCEK.Y (2^+) K.VLHALLQK.F (2^+) K.FTTSMITYIR.Y (2^+) R.DIAVQGNVDPGVLFGSK.E (2^+)	gi 14334768	43694/ 8.60	1.92 ± 0.34 ↑
11	24	unnamed protein product [*Sinapis alba*]	2/24	117/50	R.EHGSTPGYYDGR.Y (2^+) R.IIGFDNNR.Q (2^+)	gi 1345574	9768/ 6.10	23.43 ± 9.50 ↑
12	24	unnamed protein product [*S. alba*]	1/14	75/49	R.EHGSTPGYYDGR.Y (2^+)	gi 1345574	9768/ 6.10	9.11 ± 4.11 ↑
13	24	chaperonin precursor [*Pisum sativum*]	4/8	156/50	K.LADLVGVTLGPK.G (2^+) K.DTTTIVGDGSTQEAVNK.R (2^+) K.NAGVNGSVVSEK.V (2^+) K.YGYNAATGK.Y (2^+)	gi 806808	63287/ 5.85	3.13 ± 0.93 ↓
14	24	FTSH8; ATP-dependent peptidase/ ATPase/ metallopeptidase/ zinc ion binding [*A. thaliana*]	2/3	72/50	R.IVAGMEGTVMTDGK.S (2^+) K.ETMSGDEFR.A (2^+)	gi 42561751	73324/ 5.72	4.27 ± 1.56 ↑
15	24	fructose-bisphosphate aldolase [*A. thaliana*]	2/4	69/49	R.TAAYYQQGAR.F (2^+) R.ALQNTCLK.T (2^+)	gi 18399660	43075/ 6.18	2.37 ± 0.27 ↓
16	24	mRNA binding [*A. thaliana*]	5/11	156/50	R.FSEIVSGGGK.T (2^+) K.DCEEWFFDR.I (2^+) K.TVEIVHYDPK.A (2^+) K.DLLGWESK.T (2^+) K.TNLPEDLKER.F (2^+)	gi 15229384	44074/ 8.54	1.92 ± 0.22 ↓
17	24	glyceraldehyde 3-phosphate dehydrogenase B subunit [*A. thaliana*]	13/36	482/49	K.DSPLEVVVLNDSGGVK.N (2^+) K.YDSMLGTFK.A (2^+) K.IVDNETISVDGK.L (2^+) K.VLDEEFGIVK.G (2^+) K.GTMTTTHSYTGDQR.L (2^+) R.AAALNIVPTSTGAAK.A (2^+) R.AAALNIVPTSTGAAK.A (2^+) K.AVSLVLPQLK.G (2^+) R.VPTPNVSVVDLVINVEK.K (2^+) K.GLTAEDVNEAFR.K (2^+) K.VVAWYDNEWGYSQR.V (2^+) K.WPGAEAVGSGDPLEDFCK.T (2^+) K.WPGAEAVGSGDPLEDFCK.T (2^+)	gi 336390	43168/ 5.60	3.10 ± 0.73 ↓

Table 2. Continued

				ESI-q-ToF				
spot	time point (h)	protein identity	MS/MS/PM[a] (%)	score[b]	peptide sequence (charge state)	accession no.[c]	M_r/pI	fold change
18	24	methionine adenosyltransferase/ATP binding [*A. thaliana*]	10/20	262/50	R.EIGFISADVGLDADK.C (2^+) R.EIGFISADVGLDADK.C (2^+) K.NDGGAMIPIR.V (2^+) K.YLDDNTIFHLNPSGR.F (3^+) R.FVIGGPHGDAGLTGR.K (2^+) R.FVIGGPHGDAGLTGR.K (2^+) R.FVIGGPHGDAGLTGR.K (3^+) R.FVIGGPHGDAGLTGR.K (2^+) K.TGTIPDKDILVLIK.E (3^+) K.TAAYGHFGR.D (2^+)	gi 15228048	42927/ 5.76	3.65 ± 0.71 ↓
19	36	ribosomal protein L12 [*A. thaliana*]	4/16	125/49	K.IGSEISSLTLEEAR.I (2^+) K.IGSEISSLTLEEAR.I (2^+) R.ALTSLALK.E (2^+) K.ELIEGLPK.K (2^+)	gi 468773	19744/ 5.51	2.10 ± 0.27 ↑
20	36	eukaryotic translation initiation factor-5A [*B. napus*]	2/23	121/49	K.CHFVAIDIFTAK.K (2^+) K.SGFEEGKDVVVSVMSSMGEEQICAVK.E (3^+)	gi 40805177	17315/ 5.71	2.50 ± 0.59 ↓
21	36	peroxidase/ATPRXIIF/PRXIIF [*A. thaliana*]	3/15	101/49	K.FSTTPLSDIFK.G (2^+) K.DAIEFYGDFDGK.F (2^+) R.WSAYVEDGK.V (2^+)	gi 18397457	21546/ 8.99	2.33 ± 0.41 ↑
22	36	PBA1; endopeptidase/ peptidase/ threonine endopeptidase [*A. thaliana*]	4/9	168/49	K.ITQLTDNVYVCR.S (2^+) R.TVIINSEGVTR.N (2^+) R.TVIINSEGVTR.N (2^+) R.TVIINSEGVTR.N (2^+)	gi 15235889	25193/ 5.31	1.71 ± 0.28 ↑
23	36	AT4g38970/F19H22_70 [*A. thaliana*]	10/25	396/50	R.GILAMDESNATCGK.R (2^+) K.MVDVLVEQNIVPGIK.V (2^+) K.MVDVLVEQNIVPGIK.V (2^+) R.TAAYYQQGAR.F (2^+) R.TVVSIPNGPSALAVK.E (2^+) R.TVVSIPNGPSALAVK.E (2^+) R.YAAISQDSGLVPIVEPEILLDGEHDIDR.T (3^+) R.ALQNTCLK.T (2^+) K.YTGEGESEEAK.E (2^+) K.YTGEGESEEAK.E (2^+)	gi 16226653	43029/ 6.79	1.91 ± 0.32 ↓
24	36	fructose-bisphosphate aldolase [*A. thaliana*]	18/28	543/50	R.LDSIGLENTEANR.Q (2^+) R.LDSIGLENTEANR.Q (2^+) K.MVDVLVEQNIVPGIK.V (2^+) K.MVDVLVEQNIVPGIK.V (2^+) K.MVDVLVEQNIVPGIK.V (2^+) K.GLVPLVGSNNESWCQGLDGLSSR.T (2^+) K.GLVPLVGSNNESWCQGLDGLSSR.T (3^+) R.TAAYYQQGAR.F (2^+) R.YAAISQDSGLVPIVEPEILLDGEHDIDR.T (3^+) R.ATPEQVAAYTLK.L (2^+) R.ATPEQVAAYTLK.L (2^+) R.ATPEQVAAYTLK.L (2^+) K.YTGEGESEEAK.E (2^+) K.YTGEGESEEAK.E (2^+) K.YTGEGESEEAK.E (2^+) K.YTGEGESEEAK.E (2^+) K.YTGEGESEEAK.E (2^+) K.YTGEGESEEAK.E (2^+)	gi 18420348	43132/ 6.78	1.42 ± 0.13 ↓
25	48	putative glyoxalase [*Oryza sativa* (*japonica* cultivar group)]	2/6	88/41	-.MLHVVYR.V (2^+) K.FYTECLGMK.L (2^+)	gi 50933389	29720/ 4.99	3.50 ± 1.30 ↑
26	48	plastid-dividing ring protein [*Solanum tuberosum*]	3/9	198/38	K.VVGVGGGGNNAVNR.M (2^+) R.NVDTLIVIPNDR.L (2^+) K.DSGTAMLGVGVSSSK.D (2^+)	gi 47156057	44089/ 5.79	2.15 ± 0.76 ↑
27	48	RCA (rubisco activase) [*A. thaliana*]	3/9	186/38	K.MGINPIMMSAGELESGNAGEPAK.L (2^+) K.MCCLFINDLDAGAGR.M (2^+) R.VYDDEVRK.F (2^+)	gi 18405145	52347/ 5.87	2.47 ± 0.45 ↑
		plastidic glutamine synthetase precursor [*B. napus*]	8/13	175/38	K.WNYDGSSTGQAPGEDSEVILYPQAIFR.D (3^+) R.AAEIFSNK.K (2^+) R.AAEIFSNKK.V (2^+) R.EEGGFDVIK.K (2^+) R.HMEHISAYGEGNER.R (3^+) R.HMEHISAYGEGNER.R (3^+) R.HMEHISAYGEGNER.R (3^+) R.HMEHISAYGEGNER.R (3^+)	gi 1934754	47758/ 5.99	

Table 2. Continued

spot	time point (h)	protein identity	MS/MS/PM[a] (%)	ESI-q-ToF score[b]	ESI-q-ToF peptide sequence (charge state)	accession no.[c]	M_r/pI	fold change
28	48	RCA (rubisco activase) [*A. thaliana*]	4/9	189/41	K.MGINPIMMSAGELESGNAGEPAK.L (3^+) K.MGINPIMMSAGELESGNAGEPAK.L (2^+) K.MCCLFINDLDAGAGR.M (2^+) R.VYDDEVR.K (2^+)	gi 18405145	52347/ 5.87	5.32 ± 1.92 ↑
		JR1 [*A. thaliana*]	3/7	68/41	K.FDYEKDGK.I (2^+) K.TSQPFGLTSGEEAELGGGK.I (2^+) K.IVSLEHGK.Q (2^+)	gi 30684083	48524/ 5.12	
29	48	unnamed protein product [*A. thaliana*]	1/3	117/40	R.GLAYDTSDDQQDITR.G (2^+)	gi 16471	52080/ 5.80	7.89 ± 2.71 ↑
		glutamate-ammonia ligase precursor [*B. napus*]	1/3	66/40	R.HMEHISAYGEGNER.R (3^+)	gi 296223	47714/ 6.16	
30	48	ribulose-1,5-bisphosphate carboxylase/oxygenase large subunit [*B. juncea*]	3/6	60/38	K.LNYYTPEYETK.D (2^+) R.DNGLLLHIHR.A (2^+) R.ESTLGFVDLLR.D (2^+)	gi 30959088	53436/ 5.88	3.74 ± 1.07 ↑
31	48	ADP-glucose pyrophosphorylase small subunit [*B. napus*]	3/6	42/38	R.AKPAVPLGANYR.L (2^+) K.IYVLTQFNSASLNR.H (2^+) R.SAPIYTQPR.Y (2^+)	gi 7688095	57294/ 5.87	2.76 ± 0.74 ↑
32	48	proteasome-like protein α subunit [*S. tuberosum*]	2/8	111/50	K.LLQTSTSSEK.M (2^+) K.TMDSTSLTSEK.L (2^+)	gi 77999303	27293/ 5.63	4.14 ± 1.46 ↑

[a] Number of peptides matched/percent sequence coverage. [b] Mascot score for the most significant hits/Mascot cutoff (threshold score). [c] Accession numbers for proteins generated by the Mascot search.

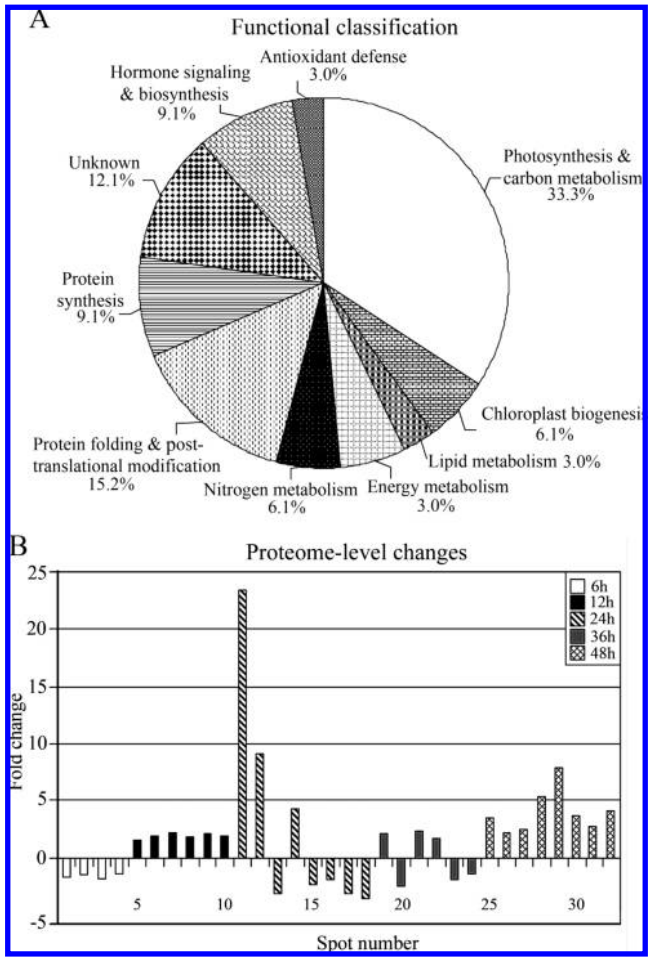

Figure 4. Functional classification (**A**) of proteins identified by tandem mass spectrometry and the fold changes in levels (**B**) following inoculation with *S. sclerotiorum*.

it has been reported that nitric oxide (NO), an essential component of certain defense-signaling cascades, is regulated by PDI (*45*). In addition, it has been reported that upon *Mycosphaerella graminicola* infection to wheat, an observed induction of PDI that occurred within 3 h was greatest in resistant lines (*46*). Chaperonins are molecular chaperones, which are present in the plastids, mitochondria, and cytoplasm of all eukaryotes and eubacteria (*47*). Chaperonins interact with other proteins and promote their assembly into functional complexes (*29*). A decrease, rather than an increase, in the intensities of spots identified as PDI and chaperonin in our studies probably reflects the susceptibility of *B. napus* to *S. sclerotiorum*. In light of the aforementioned induction of PDI in a fungi-resistant wheat line, it is possible that this gene may have utility in engineering tolerance to this devastating fungus.

Proteasome (spot 33) and other peptidases such as metallopeptidase (spot 14) and threonine endopeptidase (spot 22; **Figure 3**; **Table 2**) were also identified in our study. The 26S proteasome is a multicatalytic proteinase complex in eukaryotes that is composed of a 20S core particle (CP) that functions in proteolysis and a 19S regulatory particle (RP) that recognizes the protein targeted for degradation (*48*). The 20S proteasome consists of four seven-membered rings formed by α and β subunits (*49*). In our study, we identified the α subunit of a proteasome-like protein as being up-regulated. A role of proteasome in cell cycle progression, senescence, and the elicitation of defense responses (*50, 51*) has been reported, and the possible involvement of induced modified proteasomes known as "plant defense proteasomes" in the activation of plant defense reactions has been suggested (*48*). The increase in the intensity of the spot identified as a proteasome in this study further supports an important role for this protein in mediating plant responses to pathogens.

Antioxidant Defense and Detoxification. Plants possess complex defense mechanisms that respond to pathogen attack, including a rapid induction of antioxidant enzymes. A spot identified as the antioxidant enzyme POD was observed to be increased ~2-fold in intensity following *S. sclerotiorum* challenge (spot 21; **Figure 3**; **Table 2**). Plant POD has also been associated with a number of cellular and physiological functions,

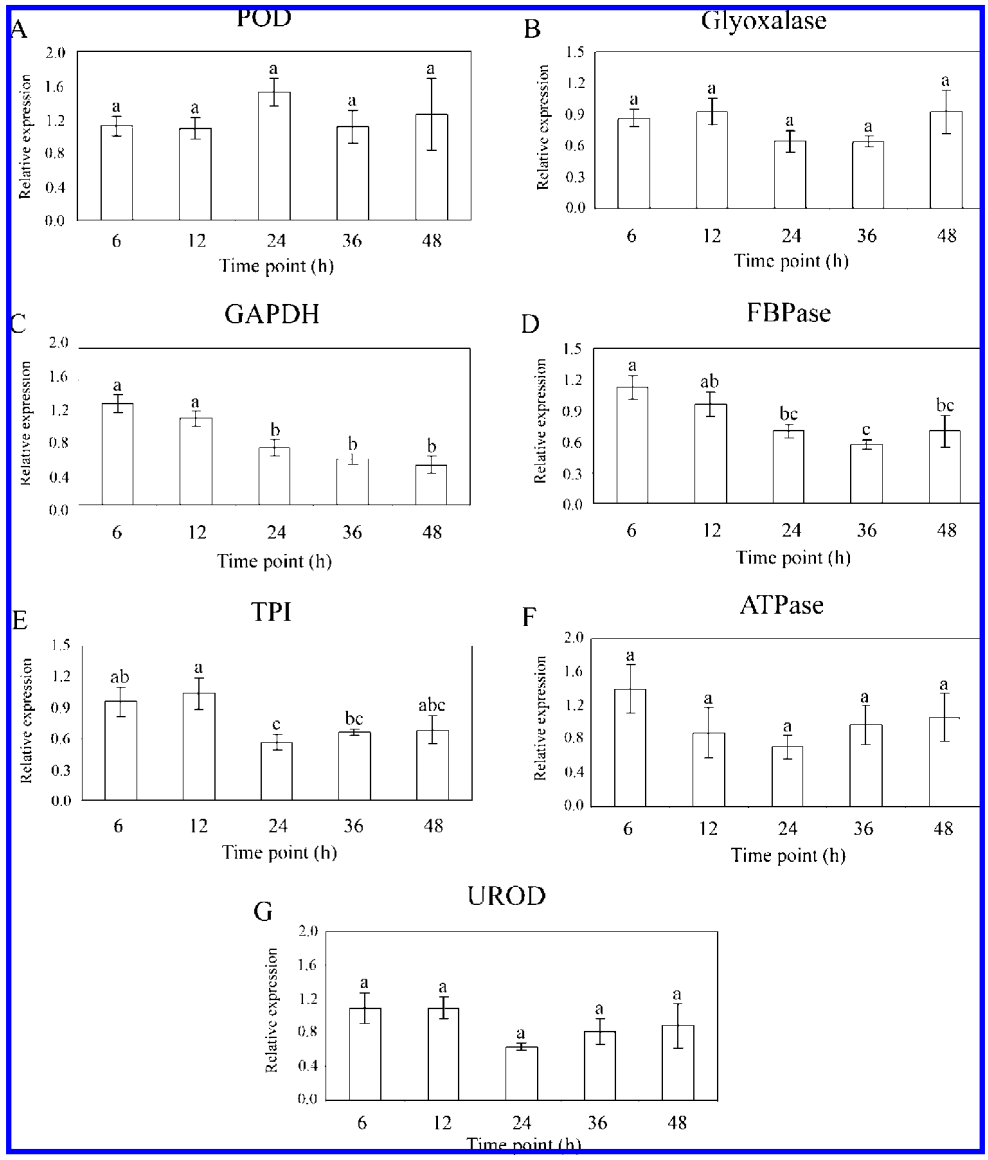

Figure 5. Changes in the relative abundance of transcripts of (**A**) POD, (**B**) glyoxalase, (**C**) GAPDH, (**D**) FBPase, (**E**) TPI, (**F**) ATPase, and (**G**) UROD at 6, 12, 24, 36, and 48 h after inoculation by *S. sclerotiorum*. All data were normalized against an actin endogenous control using the comparative C_T method (*23*), and fold changes in transcript abundance are expressed relative to the uninoculated control at the corresponding time point.

including the regulation of reactive oxygen species (ROS) by H_2O_2 removal, biosynthesis and degradation of lignin in cell walls, hormone signaling, oxidation of toxic reductants, and defense against pathogens (*52, 53*). Nevertheless, induction of PODs in host plants due to invasion of fungal pathogens has been reported in a number of studies (*52–54*); however, the presence of multiple isozymes, a lack of substrate specificity, and the complex signaling and regulatory processes involving plant peroxidases make it difficult to fully comprehend their precise physiological functions (*53, 54*). Overexpression of *POD* genes conferred enhanced abiotic stress tolerance in many plants (*54*), and antisense suppression of the expression of POD resulted in an impaired oxidative burst and susceptibility to both fungal and bacterial pathogens (*55*). It is therefore possible that plants respond to pathogen infection by increasing the cellular levels of antioxidant enzymes, including peroxidases.

To validate the role of POD in mediating *B. napus* responses to *S. sclerotiorum*, we set out to characterize the expression of a *POD* gene using qRT-PCR. Oligonucleotide primers and probes were designed on the basis of the *A. thaliana POD* sequence (due to the absence of *B. napus* sequence data); however, these primers failed to amplify *B. napus* POD. Therefore, we evaluated the response of this *POD* gene using *A. thaliana* cDNA from various time points following *S. sclerotiorum* challenge. Even though our qRT-PCR results did not show any significant changes in the abundance of this transcript, it is clear that there was an increase in transcript abundance at 24 h (**Figure 5A**). To further confirm a potential role for peroxidase in mediating responses to the pathogen, we performed peroxidase enzyme assays on crude protein extracts prepared from tissues of *B. napus*. Our results are presented in **Figure 6A** , and it is evident that peroxidase activity increased sharply and significantly ($p < 0.05$) after 24 h following inoculation. POD enzyme assay results therefore support our 2-DE gel results and further illustrate the value of proteome analysis to identify proteins (consequently genes) that may be affected as a result of a stress.

Interestingly, no other proteins associated with the antioxidant defense responses of plants were identified in our 2-DE gels, a result that is different from those reported in investigations of other pathosystems. One example is SOD, which has been implicated in a number of pathosystems (*15*). To evaluate the

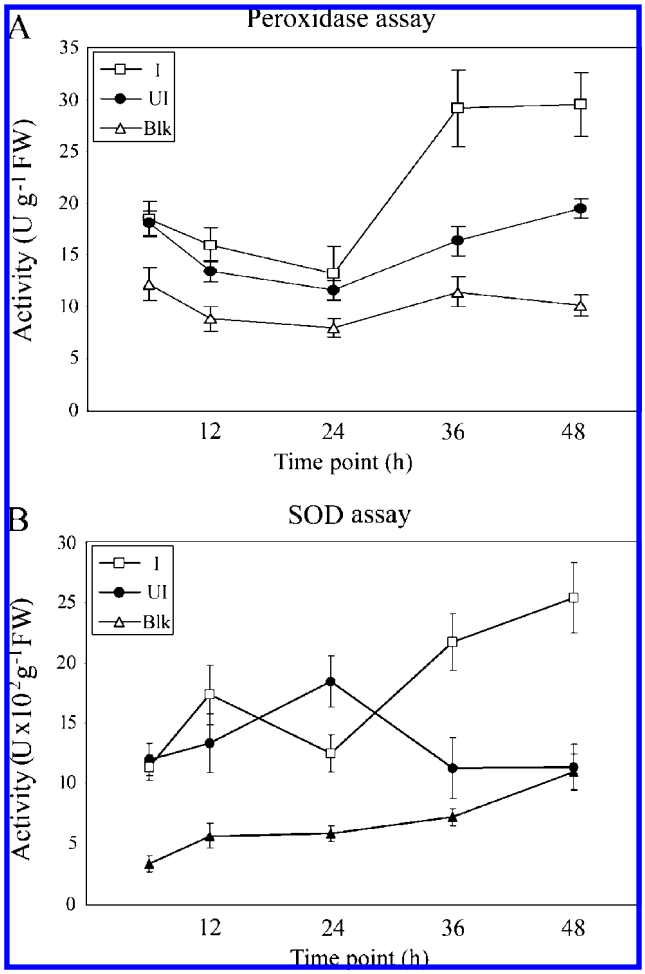

Figure 6. Peroxidase (**A**) and SOD (**B**) activity in *B. napus* leaves at 6, 12, 24, 36, and 48 h after inoculation with *S. sclerotiorum*.

role of SOD in the *B. napus*/*S. sclerotiorum* pathosystem, we performed SOD enzyme assays. The results from these assays indicated that SOD activity was significantly ($p < 0.05$) reduced at 24 h, followed by a significant ($p < 0.05$) increase in the 36–48 h time frame (**Figure 6B**). These temporal changes in the activity of SOD following inoculation with the pathogen are quite similar to those observed for POD. As mentioned earlier, it was surprising that SOD was not among the spots identified in our 2-DE gels as being significantly affected by the pathogen challenge. The discrepancy between 2-DE and enzyme assay results may be due to the fact that the observed increase in enzyme activity represents total SOD activity, whereas changes in spot intensities on 2-DE gels will be limited to the various isoforms of SOD. In other words, an individual isoform has to be elevated significantly ($p < 0.05$) for the PDQuest software to consider a spot to be significantly altered, whereas SOD enzyme assays are indicative of total activity, which appears to be significantly ($p < 0.05$; **Figure 6B**) altered in the pathogen-challenged leaf tissues. Our results suggest that POD and SOD as well as perhaps additional antioxidant enzymes are indeed elevated at 36–48 h after inoculation. However, the delayed increase in antioxidant defense responses in *B. napus* may be one of the reasons behind the successful establishment of fungal infection at earlier time points (**Figure 2**).

Another interesting enzyme identified in this study as being increased ~3-fold at 48 h after inoculation is a putative glyoxalase, more specifically, glyoxylase I (spot 25; **Figure 3**; **Table 2**). The glyoxalase system catalyzes the detoxification of methylglyoxal (MG), a toxic byproduct generated spontaneously from dihydroxyacetone phosphate, and is made up of glyoxalases I and II (*56*). MG can also accumulate as a result of the leakage of a 1,2-enediolate intermediate from the active site of TPI (*57*), or as a result of MG synthase action, and can cause numerous deleterious effects including protein degradation and modification and inactivation of antioxidant defense systems (*58*). It has also been reported that a TPI deficiency causes an increase in MG levels in infants (*59*), and it is tempting to speculate that the observed decrease in TPI has a role in increasing the MG levels during *S. sclerotiorum* infection of susceptible host species. Although the glyoxalase system has been studied extensively in response to abiotic stresses, to our knowledge, there are no papers describing the involvement (or lack thereof) of this system following infection of *B. napus* by *S. sclerotiorum*. However, a potential role for glyoxalase I has been suggested in the resistance of maize to *Aspergillus flavus (61)*, indicating the possibility that glyoxalase plays an important role in mediating plant responses during pathogen challenge. This argument is further strengthened by the increased glyoxylase I activity observed in maize lines resistant to *A. flavus* relative to that in susceptible ones (*60*).

Glyoxalases have been modulated via genetic engineering to confer salinity tolerance (*61, 62*); however, their utility in engineering disease resistance has not been demonstrated. As may be the case with the antioxidant enzymes, the timing of induction of glyoxalase in *B. napus* following pathogen challenge may determine the outcome of the interaction between host and pathogen (i.e., tolerance vs susceptibility), a suggestion that must be verified through detailed genetic and molecular approaches. In this case of *S. sclerotiorum* infection of *B. napus*, glyoxalase I appears to be induced at a later stage (48 h) and may not be able to combat the deleterious effects of methylglyoxal. To further investigate the involvement of glyoxalase I in the *B. napus*/*S. sclerotiorum* pathosystem, primers specific to the *A. thaliana* glyoxalase I gene were designed, and qRT-PCR analysis was performed. Our results indicated that glyoxalase I transcripts exhibited an increasing trend during the 36–48 h period, the timing of which paralleled the increase in the abundance of protein spot identified as glyoxylase I, suggesting a potentially important role for this enzyme. The utility of overexpressing glyoxalase to engineer tolerance to *S. sclerotiorum* (and perhaps other pathogens) is currently being investigated in our laboratory.

Proteins Involved in Hormone Biosynthesis and Signaling. Plant hormones including jasmonic acid (JA) and ethylene play important roles in mediating plant responses to stress. Both JA and ethylene signaling pathways are essential for the induction of nonspecific disease resistance, which is distinct from the salicylic acid-regulated systemic acquired resistance (SAR) (*63*). Proteins involved in ethylene biosynthesis, such as methionine adenosyltransferase (MAT; spot 18), and JA-signaling, such as JA-responsive protein (JR1; spot 6; **Figure 3**; **Table 2**), were identified in our study. MAT catalyzes the synthesis of the ethylene precursor *S*-adenosylmethionine (AdoMet) and plays an important role in mediating the cross-talk between ethylene and NO signaling pathways (*64, 65*). For example, AdoMet is a substrate for ethylene and polyamine biosynthesis, and it has been suggested that NO may regulate the ethylene biosynthesis by inhibiting MAT activity (*66*). JA has crucial roles in regulating many plant processes including mediating resistance to pathogens (*67*). JA-responsive (*JR*) genes, including *JR1*, have been demonstrated to be induced by wounding (*68*). Interest-

ingly, a recent microarray investigation into the transcriptional changes in *B. napus* following *S. sclerotiorum* challenge conducted in our laboratory revealed an increase in the transcript abundance of many JA biosynthesis-related proteins (*69*), which further supports an important role for JA in this host−pathogen pathosystem.

Validation of Transcript Abundance for Selected Genes. In addition to previously described gene expression analysis of peroxidase (**Figure 5A**) and glyoxalase (**Figure 5B**), we also investigated the relative abundance of transcripts for GAPDH, FBPase, TPI, ATPase, and UROD. For all of the genes, the primers and probes were designed on the basis of available *A. thaliana* sequence information (**Table 1**), but we were unsuccessful in using these primers to amplify the *B. napus* homologues of these genes (in all cases except ATPase) in the reverse transcriptase PCR (RT-PCR) experiments (data not shown). Because both *B. napus* and model plant *A. thaliana* are closely related and both are susceptible to *S. sclerotiorum*, exhibiting similar disease symptom development, we used *A. thaliana* cDNA from various time points after infection with *S. sclerotiorum* to perform the qRT-PCR analysis. Our qRT-PCR results indicated that GAPDH (**Figure 5C**), FBPase (**Figure 5D**), and TPI (**Figure 5E**) exhibited significant ($p < 0.05$) changes in transcript abundance following pathogen challenge. Furthermore, the changes in transcript abundance for GAPDH and FBPase exhibited a trend similar to that observed with their corresponding protein spots on 2-DE gels at the time points investigated. Contrary to these results, transcriptional analysis revealed no significant ($p < 0.05$) change for ATPase (**Figure 5F**) and UROD (**Figure 5G**). Even though the gene expression patterns for these two genes do not correlate with proteome level changes, a role for these enzymes during the response of *B. napus* to *S. sclerotiorum* cannot be ruled out due to the generally poor correlation between the transcriptome and the proteome (*13, 70*). Our 2-DE and qRT-PCR results suggest that a decrease in three Calvin cycle enzymes, GAPDH, TPI, and FBPase, may be occurring as a result of pathogen challenge, which may affect the metabolism of the pathogen-challenged plant and may have implications for the eventual outcome of the infection process. In fact, as mentioned earlier, a decrease in TPI has the potential to lead to increased MG levels, which will have deleterious consequences for the plant cell.

Global gene expression analysis using microarrays and protein analysis using proteomics are promising techniques to investigate the molecular events occurring during host−pathogen interactions. Our proteomics-based investigation of the *B. napus*/*S. sclerotiorum* pathosystem revealed the identities of many proteins that were up- or down-regulated after pathogen challenge. This is the first proteomics-based investigation of this pathosystem, and the proteins identified as increased or decreased included metabolic enzymes, as well as proteins associated with protein folding, hormone signaling, and antioxidant defense response. Furthermore, several of the proteins identified were unnamed with unknown functions. The proteomics results were validated by conducting qRT-PCR of selected genes and enzymatic activity assays for peroxidases and superoxide dismutase. Future studies will be aimed at the investigation of a link between TPI and MG detoxifying glyoxalases, which has been suggested previously (*61*) and may have utility in engineering tolerance to this pathogen.

ABBREVIATIONS USED

FBPase, fructose bisphosphate aldolase; GAPDH, glyceraldehyde-3-phosphate dehydrogenase; JR, JA-responsive; MAT, methionine adenosyltransferase; SOD, superoxide dismutase; TPI, triosephosphate isomerase; UROD, uroporphyrinogen decarboxylase.

ACKNOWLEDGMENT

We thank the Microscopy Unit at the Department of Biological Science, University of Alberta, for providing technical and material support for the histology work reported here and Nidhi Sharma for technical assistance.

LITERATURE CITED

(1) del Río, L. E.; Bradley, C. A.; Henson, R. A.; Endres, G. J.; Hanson, B. K.; McKay, K.; Halvorson, B. K.; Porter, P. M.; Le Gare, D. G.; Lamey, H. A. Impact of Sclerotinia stem rot on yield of canola. *Plant Dis.* **2007**, *91*, 191–194.

(2) Boland, G. J.; Hall, R. Index of plant hosts of *Sclerotinia sclerotiorum*. *Can. J. Plant Pathol.* **1994**, *16*, 93–108.

(3) Rimmer, S. R.; Kutcher, H. R.; Morrall, R. A. A. Diseases of canola and mustard. In *Diseases of Field Crops in Canada*; Bailey, K. L. ,Gossen, B. D., Gugel, R. K., Morrall, R. A. A., Eds.; Canadian Phytopathology Society:Saskatoon, SK, Canada, 2003; pp 129–146.

(4) Annis, S. L.; Goodwin, P. H. Recent advances in the molecular genetics of plant cell wall-degrading enzymes produced by plant pathogenic fungi. *Eur. J. Plant Pathol.* **1997**, *103*, 1–14.

(5) Cotton, P.; Kasza, Z.; Bruel, C.; Rascle, C.; Fèvre, M. Ambient pH controls the expression of endopolygalacturonase genes in the necrotrophic fungus *Sclerotinia sclerotiorum*. *FEMS Microbiol. Lett.* **2003**, *227*, 163–169.

(6) Godoy, G.; Steadman, J. R.; Dickman, M. B.; Dam, R. Use of mutants to demonstrate the role of oxalic acid in pathogenicity of *Sclerotinia sclerotiorum* on *Phaseolus vulgaris*. *Physiol. Mol. Plant Pathol.* **1990**, *37*, 179–191.

(7) Guimarães, R. L.; Stotz, H. U. Oxalate production by *Sclerotinia sclerotiorum* deregulates guard cells during infection. *Plant Physiol.* **2004**, *136*, 3703–3711.

(8) Riou, C.; Freyssinet, G.; Fevre, M. Production of cell wall-degrading enzymes by the phytopathogenic fungus *Sclerotinia sclerotiorum*. *Appl. Environ. Microbiol.* **1991**, *57*, 1478–1484.

(9) Bolton, M. D.; Thomma, B. P. H. J.; Nelson, B. D. *Sclerotinia sclerotiorum* (Lib.) de Bary: biology and molecular traits of a cosmopolitan pathogen. *Mol. Plant Pathol.* **2006**, *7*, 1–16.

(10) Yajima, W.; Kav, N. N. V. The proteome of the phytopathogenic fungus Sclerotinia sclerotiorum. *Proteomics* **2006**, *6*, 5995–6007.

(11) Li, R.; Rimmer, R.; Buchwaldt, L.; Sharpe, A. G.; Séguin-Swartz, G.; Coutu, C.; Hegedus, D. D. Interaction of *Sclerotinia sclerotiorum* with a resistant *Brassica napus* cultivar: expressed sequence tag analysis identifies genes associated with fungal pathogenesis. *Fungal Genet. Biol.* **2004**, *41*, 735–753.

(12) Liu, R.; Zhao, J.; Xiao, Y.; Meng, J. Identification of prior candidate genes for Sclerotinia local resistance in *Brassica napus* using Arabidopsis cDNA microarray and *Brassica*−*Arabidopsis* comparative mapping. *Sci. China Ser. C: Life Sci.* **2005**, *48*, 460–470.

(13) Gygi, S. P.; Rochon, Y.; Franza, B. R.; Aebersold, R. Correlation between protein and mRNA abundance in yeast. *Mol. Cell. Biol.* **1999**, *19*, 1720–1730.

(14) Kav, N. N. V.; Srivastava, S.; Goonewardene, L.; Blade, S. F. Proteome-level changes in the roots of *Pisum sativum* in response to salinity. *Ann. Appl. Biol.* **2004**, *145*, 217–230.

(15) Subramanian, S.; Bansal, V. K.; Kav, N. N. V. Proteome-level investigation of *Brassica carinata* derived resistance to *Leptosphaeria maculans*. *J. Agric. Food Chem.* **2005**, *53*, 313–324.

(16) Sharma, N.; Rahman, M. H.; Strelkov, S. E.; Thiagarajah, M.; Bansal, V. K.; Kav, N. N. V. Proteome-level changes in two *Brassica napus* lines exhibiting differential responses to the fungal pathogen *Alternaria brassicae*. *Plant Sci.* **2006**, *172*, 95–110.

(17) Jain, S.; Srivastava, S.; Sarin, N. B.; Kav, N. N. V. Proteomics reveals elevated levels of PR 10 proteins in saline-tolerant peanut (*Arachis hypogaea*) calli. *Plant Physiol. Biochem.* **2006**, *44*, 253–259.

(18) Zhou, W.; Eudes, F.; Laroche, A. Identification of differentially regulated proteins in response to a compatible interaction between the pathogen *Fusarium graminearum* and its host *Triticum aestivum*. *Proteomics* **2006**, *6*, 4599–4609.

(19) Larone, D. H. In *Medically Important Fungi: A Guide to Identification*, 3rd ed.; ASM Press: Washington, DC, 1995.

(20) Dougherty, W. J. In *Staining Procedures*, 4th ed.; George, C., Ed.; William and Wilkins: Baltimore, MD, 1981; pp 27–38.

(21) Bradford, M. M. A rapid and sensitive method for the quantitation of microgram quantities of protein utilizing the principle of protein-dye binding. *Anal. Biochem.* **1967**, *72*, 248–254.

(22) Srivastava, S.; Emery, R. J. N.; Rahman, M. H.; Kav, N. N. V. A crucial role for cytokinins in pea *ABR17*-mediated enhanced germination and early seedling growth of *Arabidopsis thaliana* under saline and low-temperature stresses. *J. Plant Growth Regul.* **2007**, *26*, 26–37.

(23) Livak, K. J.; Schmittgen, T. D. Analysis of relative gene expression data using real-time quantitative PCR and the $2\text{-}\Delta^{\Delta Ct}$ method. *Methods* **2001**, *25*, 402–408.

(24) Benkeblia, N.; Shiomi, N. Chilling effect on soluble sugars, respiration rate, total phenolics, peroxidase activity and dormancy of onion bulbs. *Sci. Agric.* **2004**, *61*, 281–285.

(25) Beauchamp, C.; Fridovich, I. Superoxide dismutase: improved assays and an assay applicable to acrylamide gels. *Anal. Biochem.* **1971**, *44*, 276–287.

(26) Giannopolitis, C. N.; Ries, S. K. Superoxide dismutases: I. Occurrence in higher plants. *Plant Physiol.* **1977**, *59*, 309–314.

(27) Babitha, M. P.; Bhat, S. G.; Prakash, H. S.; Shetty, H. S. Differential induction of superoxide dismutase in downy mildew-resistant and -susceptible genotypes of pearl millet. *Plant Pathol.* **2002**, *51*, 480–486.

(28) Lumsden, D. R.; Dow, R. L. Histopathology of *Sclerotinia sclerotiorum* infection of bean. *Phytopathology* **1973**, *63*, 708–715.

(29) Roy, H. Rubisco assembly: a model system for studying the mechanism of chaperonin action. *Plant Cell* **1989**, *1*, 1035–1042.

(30) Hanson, T. E.; Tabita, F. R. A ribulose-1,5-bisphosphate carboxylase/oxygenase (RubisCO)-like protein from *Chlorobium tepidum* that is involved with sulfur metabolism and the response to oxidative stress. *Proc. Natl. Acad. Sci. U.S.A.* **2001**, *98*, 4397–4402.

(31) Andrews, J. R.; Fryer, M. J.; Baker, N. R. Characterization of chilling effects on photosynthetic performance of maize crops during early season growth using chlorophyll fluorescence. *J. Exp. Bot.* **1995**, *46*, 1195–1203.

(32) Portis, A. R., Jr.; Lilley, R. M.; Andrews, T. J. Subsaturating ribulose-1,5-bisphosphate concentration promotes inactivation of ribulose-1,5-bisphosphate carboxylase/oxygenase (rubisco) (studies using continuous substrate addition in the presence and absence of rubisco activase). *Plant Physiol.* **1995**, *109*, 1441–1451.

(33) Kleczkowski, L. A. Is leaf ADP-glucose pyrophosphorylase an allosteric enzyme. *Biochim. Biophys. Acta* **2000**, *1476*, 103–108.

(34) Sanwal, G. G.; Greenberg, E.; Hardie, J.; Cameron, E. C.; Preiss, J. Regulation of starch biosynthesis in plant leaves: activation and inhibition of ADPglucose pyrophosphorylase. *Plant Physiol.* **1968**, *43*, 417–427.

(35) Mock, H. P.; Heller, W.; Molina, A.; Neubohn, B.; Sandermann, H., Jr.; Grimm, B. Expression of uroporphyrinogen decarboxylase or coproporphyrinogen oxidase antisense RNA in tobacco induces pathogen defense responses conferring increased resistance to tobacco mosaic virus. *J. Biol. Chem.* **1999**, *274*, 4231–4238.

(36) Pageau, K.; Reisdorf-Cren, M.; Morot-Gaudry, J. F.; Masclaux-Daubresse, C. The two senescence-related markers, GS1 (cytosolic glutamine synthetase) and GDH (glutamate dehydrogenase), involved in nitrogen mobilization, are differentially regulated during pathogen attack and by stress hormones and reactive oxygen species in *Nicotiana tabacum* L. leaves. *J. Exp. Bot.* **2006**, *57*, 547–557.

(37) Zörb, C.; Schmitt, S.; Neeb, A.; Karl, S.; Linder, M.; Schubert, S. The biochemical reaction of maize (*Zea mays* L.) to salt stress is characterized by a mitigation of symptoms and not by a specific adaptation. *Plant Sci.* **2004**, *167*, 91–100.

(38) Stephenson, S. A.; Green, J. R.; Manners, J. M.; Maclean, D. J. Cloning and characterisation of glutamine synthetase from *Colletotrichum gloeosporioides* and demonstration of elevated expression during pathogenesis on *Stylosanthes guianensis*. *Curr. Genet.* **1997**, *31*, 447–454.

(39) Rampitsch, C.; Bykova, N. V.; McCallum, B.; Beimcik, E.; Ens, W. Analysis of the wheat and *Puccinia triticina* (leaf rust) proteomes during a susceptible host-pathogen interaction. *Proteomics* **2006**, *6*, 1897–1907.

(40) Langston-Unkefer, P. J.; Robinson, A. C.; Knight, T. J.; Durbin, R. D. Inactivation of pea seed glutamine synthetase by the toxin, tabtoxinine-β-lactam. *J. Biol. Chem.* **1987**, *262*, 1608–1613.

(41) Ochs, G.; Schock, G.; Trischler, M.; Kosemund, K.; Wild, A. Complexity and expression of the glutamine synthetase multigene family in the amphidiploid crop *Brassica napus*. *Plant Mol. Biol.* **1999**, *39*, 395–405.

(42) Ellis, R. J.; Hemmingsen, S. M. Molecular chaperones: proteins essential for the biogenesis of some macromolecular structures. *Trends Biochem. Sci.* **1989**, *14*, 339–342.

(43) Wilkinson, B.; Gilbert, H. F. Protein disulfide isomerase. *Biochim. Biophys. Acta* **2004**, *1699*, 35–44.

(44) Schultz-Norton, J. R.; McDonald, W. H.; Yates, J. R.; Nardulli, A. M. Protein disulfide isomerase serves as a molecular chaperone to maintain estrogen receptor alpha structure and function. *Mol. Endocrinol.* **2006**, *20*, 1982–1995.

(45) Zai, A.; Rudd, M. A.; Scribner, A. W.; Loscalzo, J. Cell-surface protein disulfide isomerase catalyzes transnitrosation and regulates intracellular transfer of nitric oxide. *J. Clin. Invest.* **1999**, *103*, 393–399.

(46) Ray, S.; Anderson, J. M.; Urmeev, F. I.; Goodwin, S. B. Rapid induction of a protein disulfide isomerase and defense-related genes in wheat in response to the hemibiotrophic fungal pathogen *Mycosphaerella graminicola*. *Plant Mol. Biol.* **2003**, *53*, 741–754.

(47) Hill, J. E.; Hemmingsen, S. M. *Arabidopsis thaliana* type I and II chaperonins. *Cell Stress Chaperon.* **2001**, *6*, 190–200.

(48) Suty, L.; Lequeu, J.; Lancon, A.; Etienne, P.; Petitot, A. S.; Blein, J. P. Preferential induction of 20S proteasome subunits during elicitation of plant defense reactions: towards the characterization of "plant defense proteasomes". *Int. J. Biochem. Cell Biol.* **2003**, *35*, 637–650.

(49) Baumeister, W.; Walz, J.; Zuhl, F.; Seemuller, E. The proteasome: paradigm of a self-compartmentalizing protease. *Cell* **1998**, *92*, 367–380.

(50) Conrath, U.; Klessig, D. F.; Bachmair, A. Tobacco plants perturbed in the ubiquitin-dependent protein degradation system accumulate callose, salicylic acid, and pathogenesis-related protein 1. *Plant Cell Rep.* **1998**, *17*, 876–880.

(51) Ito, N.; Seo, S.; Ohtsubo, N.; Nakagawa, H.; Ohashi, Y. Involvement of proteasome−ubiquitin system in wound-signaling in tobacco plants. *Plant Cell Physiol.* **1999**, *40*, 355–360.

(52) Fossdal, C. G.; Sharma, P.; Lonneborg, A. Isolation of the first putative peroxidase cDNA from a conifer and the local and systemic accumulation of related proteins upon pathogen infection. *Plant Mol. Biol.* **2001**, *47*, 423–435.

(53) Yoshida, K.; Kaothien, P.; Matsui, T.; Kawaoka, A. Molecular biology and application of plant peroxidase genes. *Appl. Microbiol. Biotechnol.* **2003**, *60*, 665–670.

(54) Curtis, M. D.; Rae, A. L.; Rusu, A. G.; Harrison, S. J.; Manners, J. M. A peroxidase gene promoter induced by phytopathogens and methyl jasmonate in transgenic plants. *Mol. Plant Microbe. Interact.* **1997**, *10*, 326–338.

(55) Bindschedler, L. V.; Dewdney, J.; Blee, K. A.; Stone, J. M.; Asai, T.; Plotnikov, J.; Denoux, C.; Hayes, T.; Gerrish, C.; Davies, D. R.; Ausubel, F. M.; Bolwell, G. P. Peroxidase-dependent apoplastic oxidative burst in *Arabidopsis* required for pathogen resistance. *Plant J.* **2006**, *47*, 851–863.

(56) Thornalley, P. J. The glyoxalase system: new developments towards functional characterization of a metabolic pathway fundamental to biological life. *Biochem. J.* **1990**, *269*, 1–11.

(57) Richard, J. P. Kinetic parameters for the elimination reaction catalyzed by triosephosphate isomerase and an estimation of the reaction's physiological significance. *Biochemistry* **1991**, *30*, 4581–4585.

(58) Martins, A. M. T. B. S.; Cordeiro, C. A. A.; Freire, A. M. J. P. In situ kinetic analysis of glyoxalase I and glyoxalase II in *Saccharomyces cerevisiae*. *FEBS Lett.* **2001**, *499*, 41–44.

(59) Ahmed, N.; Battah, S.; Karachalias, N.; Babaei-Jadidi, R.; Horányi, M.; Baróti, K.; Hollan, S.; Thornalley, P. J. Increased formation of methylglyoxal and protein glycation, oxidation and nitrosation in triosephosphate isomerase deficiency. *Biochim. Biophys. Acta* **2003**, *1639*, 121–132.

(60) Chen, Z. Y.; Brown, R. L.; Damann, K. E.; Cleveland, T. E. Identification of a maize kernel stress-related protein and its effects on aflatoxin accumulation. *Phytopathology* **2004**, *94*, 938–945.

(61) Singla-Pareek, S. L.; Yadav, S. K.; Pareek, A.; Reddy, M. K.; Sopory, S. K. Enhancing salt tolerance in a crop plant by overexpression of glyoxalase II. *Transgenic Res.* **2007**,DOI 10.1007/s11248-007-9082-2.

(62) Veena; Reddy, V. S.; Sopory, S. K. Glyoxalase I from *Brassica juncea*: molecular cloning, regulation and its over-expression confer tolerance in transgenic tobacco under stress. *Plant J.* **1999**, *17*, 385–395.

(63) Dong, X. SA, JA, ethylene, and disease resistance in plants. *Curr. Opin. Plant Biol.* **1998**, *1*, 316–323.

(64) Delledonne, M.; Xia, Y.; Dixon, R. A.; Lamb, C. Nitric oxide functions as a signal in plant disease resistance. *Nature* **1998**, *394*, 585–588.

(65) Lindermayr, C.; Saalbach, G.; Bahnweg, G.; Durner, J. Differential inhibition of *Arabidopsis* methionine adenosyltransferases by protein S-nitrosylation. *J. Biol. Chem.* **2006**, *281*, 4285–4291.

(66) Wang, Y.; Yun, B. W.; Kwon, E.; Hong, J. K.; Yoon, J.; Loake, G. J. S-Nitrosylation: an emerging redox-based post-translational modification in plants. *J. Exp. Bot.* **2006**, *57*, 1777–1784.

(67) Creelman, R. A.; Mullet, J. E. Biosynthesis and action of jasmonates in plants. *Annu. Rev. Plant Physiol. Plant Mol. Biol.* **1997**, *48*, 355–381.

(68) León, J.; Rojo, E.; Titarenko, E.; Sánchez-Serrano, J. J. Jasmonic acid-dependent and -independent wound signal transduction pathways are differentially regulated by Ca^{2+}/calmodulin in *Arabidopsis thaliana*. *Mol. Gen. Genet.* **1998**, *258*, 412–419.

(69) Yang, B.; Srivastava, S.; Deyholos, M. K.; Kav, N. N. V. Transcriptional profiling of canola (*Brassica napus* L.) responses to the fungal pathogen *Sclerotinia sclerotiorum*. *Plant Sci.* **2007**, *173*, 156–171.

(70) Greenbaum, D.; Colangelo, C.; Williams, K.; Gerstein, M. Comparing protein abundance and mRNA expression levels on a genomic scale. *Genome Biol.* **2003**, *4*, 117124.

Received for review October 12, 2007. Revised manuscript received January 10, 2008. Accepted January 19, 2008. Financial assistance from the Natural Sciences and Engineering Research Council (NSERC) of Canada, the Alberta Agricultural Research Institute (AARI), the University of Alberta, the A. W. Henry Endowment Fund, and the China Scholarship Council (CSC) is gratefully acknowledged.

JF073012D